Cancer Nanotechnology

RESEARCH Open Access

Non-small cell lung cancer targeted nanoparticles with reduced side effects fabricated by flash nanoprecipitation

Mingwei Wang[1], Haiyan Huang[1], Zilong Zhong[1], Xinyue Chen[1], Yuan Fang[1], Shenxin Chen[1], Zhiyao Qi[1], Danrong Yang[2], Junyou Wang[1*] and Wei Bian[2*]

*Correspondence: junyouwang@ecust.edu.cn; bianweily@163.com

[1] Shanghai Key Laboratory of Multiphase Materials Chemical Engineering, School of Chemical Engineering, East China University of Science and Technology, Shanghai 200237, People's Republic of China
[2] Department of Respiratory Medicine, Shanghai Sixth People's Hospital Affiliated to Shanghai Jiao Tong University School of Medicine, Shanghai 200233, People's Republic of China

Abstract

Background: Tyrosine kinase inhibitors (TKI) have been highlighted for the therapy of non-small-cell lung cancer (NSCLC), due to their capability of efficiently blocking signal pathway of epidermal growth factor receptor (EGFR) which causes the inhibition and apoptosis of NSCLC cells. However, EGFR-TKIs have poor aqueous solubility and severe side effects arising from the difficulty in control of biodistribution. In this study, folate-functionalized nanoparticles (FA-NPs) are designed and fabricated to load EGFR-TKI through flash nanoprecipitation (FNP) strategy, which could enhance the tumor-targeting drug delivery and reduced drug accumulation and side effects to normal tissues.

Results: Herein, the EGFR-TKI loaded FA-NPs are constructed by FNP, with FA decorated dextran-*b*-polylactide as polymeric stabilizer and gefitinib as TKI. The fast mixing and co-precipitation in FNP provide FA-NPs with well-defined particle size, narrow size distribution and high drug loading content. The FA-NPs exhibit efficient uptake and cytotoxicity in HCC827 NSCLC cells, and reduced uptake and cytotoxicity in normal cells comparing with free gefitinib. In vivo evaluation of gefitinib-loaded FA-NPs confirms the selective drug delivery and accumulation, leading to enhanced inhibition on NSCLC tumor and simultaneously diminished side effects to normal tissues.

Conclusion: The facile design of FA-NPs by FNP and their achieved performance in vitro and in vivo evaluations offer new therapeutic opportunities for treatment of non-small cell lung cancer.

Keywords: NSCLC, Flash nanoprecipitation, Drug-loaded nanoparticles, Targeting delivery, Tyrosine kinase inhibitors, Reduced side effects

Graphical Abstract

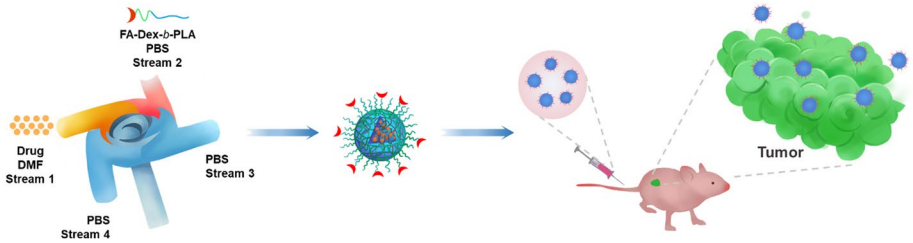

Background

Lung cancer is a leading cause of cancer-related death worldwide. About 85% of the most malignant cases is the non-small-cell lung cancer (NSCLC), which is usually induced by genetic instability arising from the tobacco (Devarakonda and Govindan 2019; Jin et al. 2021; Siegel et al. 2022). The initiation of NSCLC involves the constitutive activation of a transmembrane receptor tyrosine kinase protein, namely epidermal growth factor receptor (EGFR). The overexpression of EGFR leads to the proliferation, progression, metastasis and poor prognosis of tumor cells (Heigener et al. 2019; Meador et al. 2021). Thus, the EGFR-targeted inhibitors to block the EGFR signaling pathways, such as tyrosine kinase inhibitor (TKI), demonstrates an effective strategy for NSCLC treatment (Murtuza et al. 2019; Zhang et al. 2019). For example, gefitinib and afatinib are FDA approved TKIs that have been applied widely for inhibition and apoptosis of NSCLC cells (Maemondo et al. 2010; Tan et al. 2020). However, these inhibitors have poor aqueous solubility and short blood circulation lifetime that give problems for drug administration. More notably, control of the biodistribution of inhibitors is rather difficult, and the accumulation of inhibitors in normal tissues leads to serious side effects covering liver injury, gastrointestinal perforation, renal dysfunction, etc. (Bertran-Alamillo et al. 2019; Yuan et al. 2020).

Designing drug-loaded nanoparticles (NPs) demonstrates a prospective approach to address the application limitations of EGFR-TKIs. Particularly, polymeric NPs provide not only the enhanced solubility and prolonged circulation of hydrophobic drugs, but also extravasate to tumor sites due to the enhanced permeability and retention (EPR) effect (Behzadi et al. 2017; Besford et al. 2020; Popov et al. 2022; Seidi et al. 2018; Sousa De Almeida et al. 2021). Moreover, the surface of polymeric NPs could be functionalized with "bioactive" or tumor-targeting molecules, such as folate (FA), to further improve the accumulation of drug in tumor site, and preferably reduce side effects to normal tissues (Liu et al. 2016; Shi et al. 2014; Yang et al. 2018). Anti-solvent precipitation is a widespread strategy applied for preparing EGFR-TKI loaded polymeric NPs, while unfortunately, most of the reports so far focus on conventional precipitation methods that rely on spontaneously co-assembly of drug and stabilizing polymers and the drug is encapsulated inside the polymer shell (Akbulut et al. 2009; D'Addio and Prud'Homme 2011; Zhang et al. 2022). This time-consuming process normally creates thermodynamic controlled NPs with low yield and drug loading content (Saad and Prud'Homme 2016; Tao et al. 2019).

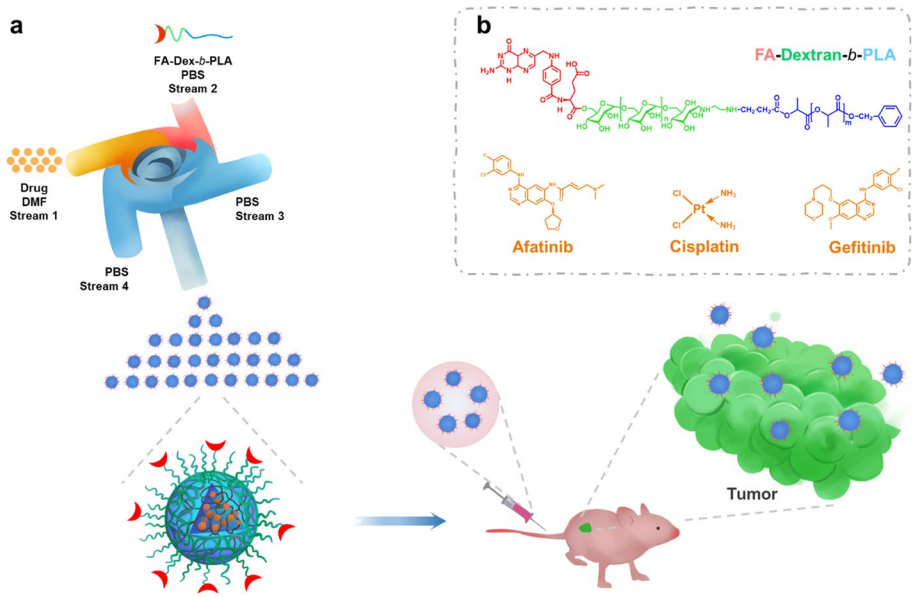

Scheme 1 **a** Illustration of EGFR-TKI loaded NPs fabrication by FNP and their performance on the therapy of NSCLC tumor. Streams containing TKIs and polymer stabilizer are mixed on MIVM (multiple inlet vortex mixer) and construct well-defined EGFR-TKI loaded NPs. **b** Chemical structures of drugs including afatinib, cisplatin and gefitinib, and the polymer stabilizer Dextran-*b*-PLA decorated with FA

Herein, we employ a fast precipitation strategy, namely flash nanoprecipitation (FNP) to prepare EGFR-TKI loaded NPs (Hu et al. 2021; Johnson and Prud'Homme 2003a, 2003b; Zhu et al. 2019). FNP relies on rapid mixing of solvent streams containing different precursor solutes based on either confined impingement jets mixers (CIJM) or multiple inlet vortex mixers (MIVM) (Liu et al. 2020; Wang et al. 2015; Zhu 2013). Mixing in these devices happens on the order of milliseconds, and the triggered co-precipitation of the drug molecules and protecting macromolecules creates kinetically controlled nanoparticles (Liu et al. 2007; Wang et al. 2018a, b; York et al. 2012). Previous studies have validated that FNP achieves great success on construction of drug-loaded polymer nanoparticles in a continuous and controllable manner (He et al. 2017; Liu et al. 2015; Santos et al. 2016; Wang et al. 2018a, b). Hence in this study, we extend this FNP strategy to fabricate EGFR-TKI loaded NPs, with aim of addressing the fabrication limitations of conventional precipitation methods. Meanwhile, we implement in vitro and in vivo study of the NPs on the bio-medical application. As shown in Scheme 1, afatinib, cisplatin and gefitinib are selected as drugs, dextran-*b*-polylactide decorated with FA ligand (FA-Dextran-*b*-PLA) is applied as the polymer stabilizer. We demonstrate that, manipulating drug and polymer molecules enable efficient preparation of EGFR-TKI loaded FA-NPs with well-defined particle size and narrow size distribution, high drug loading content and stability. Further in vitro and in vivo tests reveal that, gefitinib-loaded FA-NPs lead to selective biodistribution, and consequently enhanced drug accumulation and inhibition in NSCLC tumor, while reduced drug collection and side effects in normal tissues with respect to free drug. The achieved performance is assigned to the regulated properties of NPs fabricated by FNP, which demonstrates an advanced strategy for fabricating EGFR-TKI loaded NPs for therapeutic nanoplatform for NSCLC.

Results and discussion

Preparation of EGFR-TKI loaded FA-NPs by FNP

The EGFR-TKI loaded NPs are fabricated by FNP strategy, as illustrated in Scheme 1. FA ligand is employed for targeting the NSCLC cells, through the high folate-binding affinity of the over-expressed folate receptor (FRα) on NSCLC cells (Muralidharan et al. 2016; Pi et al. 2018; Yin et al. 2019). The dextran-based amphiphilic block copolymer Dextran-*b*-PLA is chosen as the polymeric stabilizer due to its biocompatibility (Additional file 1: Fig. S1) (Breitenbach et al. 2017; Miao et al. 2018; Schatz et al. 2009). FA ligand is grafted on the dextran chain through an esterification reaction between the γ-activated carboxyl group of FA and the abundant hydroxyl group of dextran, and the calculated decoration degree of FA is 3.7% (Additional file 1: Fig. S2). Afatinib is applied first as the EGFR-TKI. To prepare afatinib-loaded FA-NPs, afatinib is dissolved in DMF at 2 mg/mL (stream 1), and FA-Dextran-*b*-PLA is dissolved in PBS buffer (2 mg/mL, stream 2); stream 3 and 4 contains PBS buffer solutions. The mixing of the different streams and the subsequent formation of NPs are realized in MIVM by syringe pump with controlled stream velocity: stream 1 and stream 2 enter the MIVM at velocities of 10 mL/min, while stream 3 and stream 4 flow at velocities of 100 mL/min. Meanwhile, we also prepared afatinib-loaded FA-NPs by conventional anti-solvent precipitation method under the same drug/polymer combination and final concentration, serving as a control sample.

We first investigate the size and size distribution of afatinib-loaded FA-NPs from different precipitation methods by light scattering results. As shown in Fig. 1a, FA-NPs from FNP have a hydrodynamic radius (R_h) around 140 nm and a narrow size distribution (PDI ~ 0.24), whereas particles from conventional precipitation show larger spread

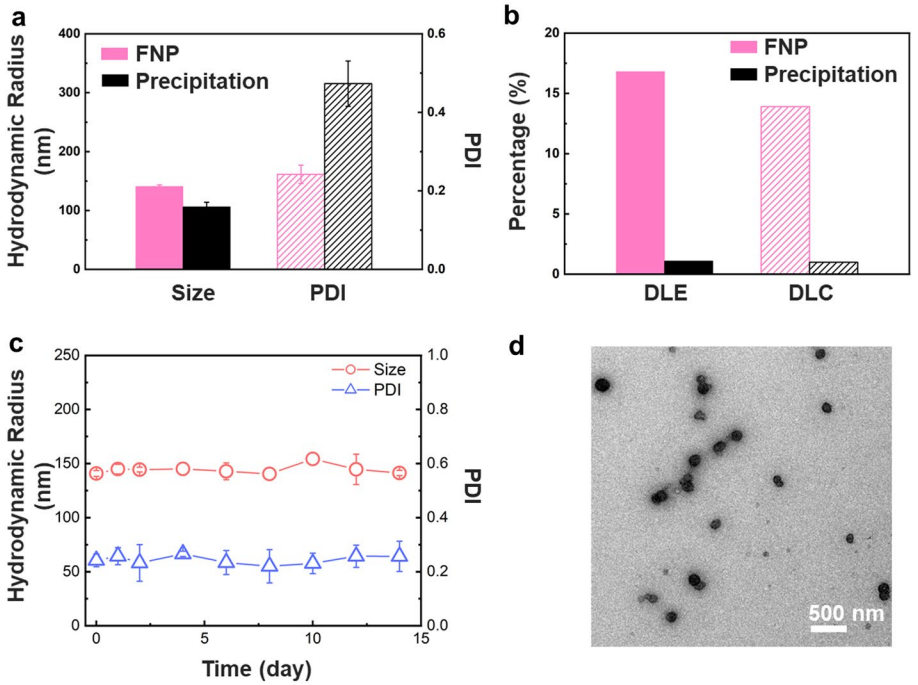

Fig. 1 **a** Size and size distribution; **b** DLE and DLC of afatinib-loaded FA-NPs prepared by FNP and conventional precipitation method; **c** stability of size and PDI at 4 °C; **d** TEM images of afatinib-loaded FA-NPs prepared by FNP

in size (PDI ~ 0.48). Moreover, drug loading efficiency (DLE) and drug loading content (DLC) of FA-NPs from FNP are about 16.8% and 13.9%, which are much higher than these values for NPs from conventional precipitation (1.1% and 1.0%, respectively), as shown in Fig. 1b. In addition, the size and PDI of FA-NPs prepared by FNP hardly change at 4 °C over 2 weeks (Fig. 1c), demonstrating an adequate storage stability. The morphology of FA-NPs prepared by FNP is further confirmed by TEM (Fig. 1d). The estimated diameter of the NPs is around 205 nm for TEM on average with spherical shape, which is smaller to the light scattering results (R_h ~ 140 nm, that is, diameter ~ 280 nm). The larger size in DLS could be attributed to the fact of that DLS provides an R_h value including the dextran shell in the hydration state. In view of these findings, we conclude that, FNP is more favorable for preparing FA-NPs with lower PDI and higher drug loading efficiency.

In addition, to extend this strategy as a general fabrication method, another EGFR-TKI gefitinib and an anti-cancer drug (cisplatin) are further employed as the drug for prepared the FA-NPs. As shown in Fig. 2a and Additional file 1: Fig. S3, gefitinib-loaded and cisplatin-loaded FA-NPs show R_h around 70 nm and 158 nm, respectively. Both are spherical nanoparticles with narrow size distribution (PDI ~ 0.25). Moreover, DLE and DLC of gefitinib-loaded NPs are about 18.9% and 15.9%, while by contrast the DLC for cisplatin-loaded NPs is lower about 7.8% (Fig. 2b). Both FA-NPs remain stable over 2 weeks with barely changed sizes as shown in Fig. 2c. On the other hand, the in vitro drug release behaviors of all three kinds of drug-loaded FA-NPs are evaluated at pH 6.5 and 7.4, which might simulate tumor extracellular and normal tissue (Additional file 1: Fig. S4). All the drug-loaded FA-NPs display similar release profiles in the PBS medium at different pH: initial fast drug release stage and later stable release stage. Comparing with afatinib-loaded FA-NPs and cisplatin-loaded FA-NPs, gefitinib-loaded FA-NPs release more drugs up to 77% at pH 6.5 and 74% at pH 7.4, which are higher than the values of released afatinib and cisplatin (50–60%). In the following, we employ gefitinib-loaded FA-NPs for the further investigation in vitro and in vivo due to the relatively high DLC and smaller size.

Cellular uptake, cytotoxicity and proliferation inhibition

The targeting cellular uptake of NSCLC cells is the key design of EGFR-TKI loaded FA-NPs. Here, to investigate the targeting behavior of FA-NPs to cancer cells, the HCC827 NSCLC cell lines are used, and HL-7702 normal liver cell lines are selected as normal cell line. Meanwhile, to evaluate the effect of FA-ligand induced cancer cell targeting

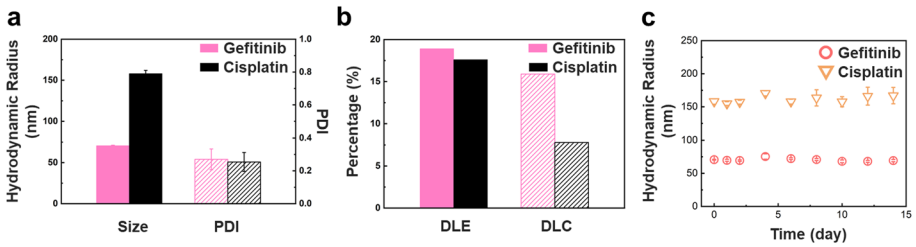

Fig. 2 **a** Size and size distribution, **b** DLE and DLC, and **c** stability of gefitinib-loaded FA-NPs and cisplatin-loaded FA-NPs

and selective uptake, the non-targeted NPs (without folate ligand, gefitinib-loaded NPs formed by Dextran-*b*-PLA) is employed as control sample as well, which is prepared at the same condition by FNP with comparable size, distribution and drug loading (Additional file 1: Table S2). Here, the phagocytic ratio (%) is introduced as the ratio of gefitinib-containing cells to total cells. As shown in Fig. 3a and Additional file 1: Fig. S5, FA-NPs are efficient in entering the NSCLC cells, 90% phagocytic ratio is reached within 6 h and finally almost 100% phagocytic ratio is achieved within 24 h, which is similarly to the free gefitinib. NPs without FA group show much lower phagocytic ratio and slower uptake rate. While by contrast, for the HL-7702 normal liver cell case, FA-NPs display much lower cellular uptake (46.9%) which is only around half of free gefitinib (81.2%) within 24 h. This value is similar to NPs without FA ligand (43.9%) as shown in Fig. 3b and Additional file 1: Fig. S5. These results indicate the high affinity and the selective cellular uptake of FA-NPs for targeting NSCLC cells.

The in vitro cytotoxicity of FA-NPs is then evaluated against HCC827 NSCLC cells after 48 h treatment with free gefitinib, FA-Dextran-b-PLA polymer, NPs and FA-NPs (Fig. 3c). The results reveal that FA-Dextran-b-PLA polymer is not toxic to HCC827 cell lines, even at concentrations up to 50 μmol/L. In contrast, the inhibition of NSCLC cells growth is observed when they are treated with gefitinib with different formations. FA-NPs show higher cytotoxicity than free gefitinib, due to the FR-mediated endocytosis: the half-maximal inhibitory concentration (IC 50) of FA-NPs against HCC827 cells is 1.08 ± 0.09 μmol/L, which is lower than the value of free gefitinib (3.96 ± 0.21 μmol/L).

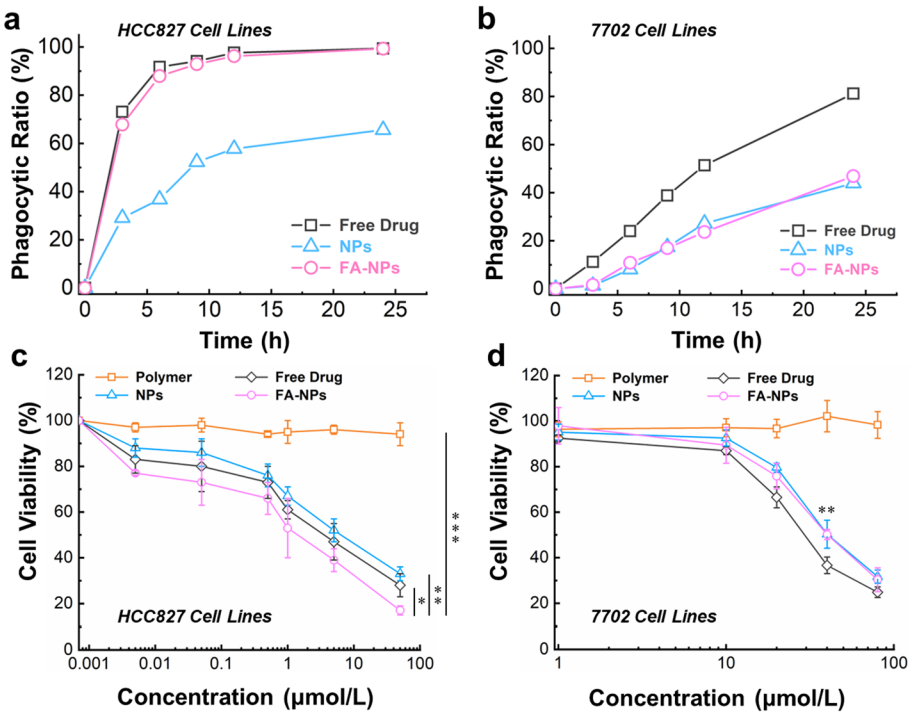

Fig. 3 Plot of the cellular uptake of **a** HCC827 NSCLC cell lines and **b** HL7702 normal liver cell lines, incubated with free drug, NPs and FA-NPs against different periods of time. Cytotoxicity to **c** HCC827 NSCLC cell lines, **d** HL7702 normal cell lines after incubation with free drug, NPs and FA-NPs, at different gefitinib concentrations after incubation of 48 h. **P* < 0.05, ***P* < 0.01 and ****P* < 0.001, compared between the indicated groups

However, NPs group exhibit less toxicity than both of free gefitinib and FA-NPs, possibly due to the low cellular uptake of NSCLC, which is consistent with the phagocytic ratio results in Fig. 3a. On the other hand, FA-NPs show relatively higher cell viability than free gefitinib in either HL7702 liver normal cells or 293 T kidney normal cells, similar with polymer (Fig. 3d and Additional file 1: Fig. S6). In view of these findings, FA-NPs is a suitable platform for the selective yet efficient inhibition of NSCLC cells.

Biodistribution

The selective cellular uptake of the FA-NPs in vitro encouraged us to further study their performances in vivo. The biodistribution of FA-NPs and free gefitinib are carried out in HCC827-tumor-bearing nude mice. The mice are killed after injection in designed time intervals, and organs are collected to determine gefitinib contents in plasma, liver, kidney, and tumor. First, the concentrations of gefitinib in plasma are detected after intravenous administration. As shown in Fig. 4a, FA-NPs exhibit notably higher concentration in plasma and prolonged blood circulation comparing with free gefitinib, owing to the shadowing effect of the nano-carrier shell (Blanco et al. 2015; Zheng et al. 2021). Moreover, reduced liver and kidney accumulation of gefitinib, associated with enhanced tumor accumulation, are observed in the FA-NPs group which is attributed to the active targeting by FRα recognition of NSCLC cancer cell and passive EPR effect during prolonged circulation (Fig. 4b). These results demonstrate that the FA-NPs endow a selectively yet favorable biodistribution of drugs, that is, enhanced accumulation in NSCLC tumor and reduced collection in normal tissue.

Anticancer effects in vivo

Anti-tumor assessments are carried out to demonstrate the therapeutic efficacy of FA-NPs. HCC827-tumor-bearing nude mice with tumor volumes of ~ 100 mm^3 are randomly divided into three groups ($n = 5$ per group), and then they are injected with gefitinib-loaded FA-NPs, free gefitinib and PBS (control) via the tail vein every two days. The changes in tumor volumes and body weights of the mice during treatments are shown in Fig. 5a and b. Therapeutic effects are observed in both of FA-NPs and free gefitinib groups, not with the control group.

As displayed in Fig. 5a, c and d, tumor volume on 16th day notably decreased in response to the therapy of gefitinib-loaded FA-NPs and free gefitinib, in comparison to

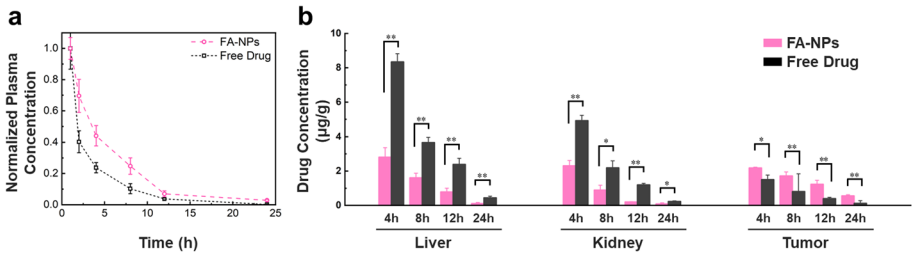

Fig. 4 Biodistribution of gefitinib in vivo. **a** Normalized concentrations of gefitinib in plasma (in FA-NPs or free form); **b** tissue distributions of gefitinib in HCC827-tumor-bearing nude mice after intravenous injection of FA-NPs or free gefitinib for designed time intervals. *$P < 0.05$ and **$P < 0.01$, compared between the indicated groups

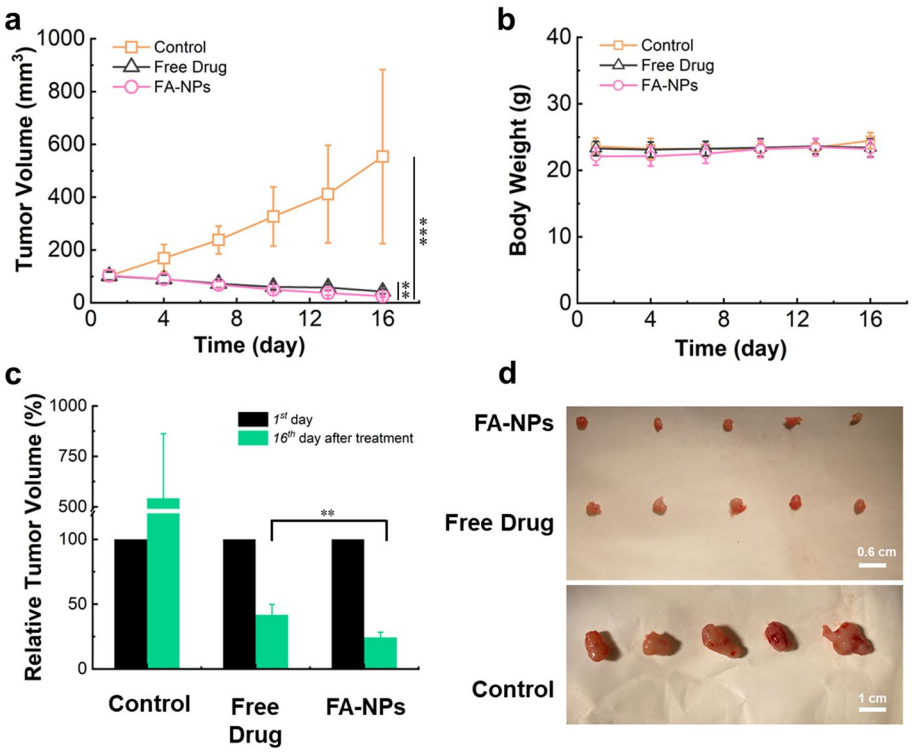

Fig. 5 Anti-tumor effects in vivo. **a** Tumor growth curves, and **b** body weight changes of HCC827-tumor-bearing nude mice after treatment with FA-NPs, free drug or PBS ($n = 5$); **c** inhibition on tumor volume; **d** photograph of tumors on 16th day after treatment. $^{**}P < 0.01$ and $^{***}P < 0.001$, compared between the indicated groups

PBS group. The tumor volumes of the mice injected with PBS increased from ~ 100 to ~ 550 mm^3 with relative tumor volume rates ~ 542% on 16th day, indicating no antitumor efficacy. While by contrast, the tumor volumes of mice treated with free gefitinib alone decrease from ~ 100 to ~ 42 mm^3 with relative tumor volume rates ~ 41.8%, showing that gefitinib could exert an obvious effect in inhibiting the proliferation of HCC827 cells. Mice treated with gefitinib-loaded FA-NPs show a better control on tumor than free drug: the tumor volume decreases of from ~ 100 to ~ 25 mm^3 with relative tumor volume rates ~ 24.3% on 16th day. On the other hand, the body weights of mice in FA-NPs groups increase a little bit from ~ 22.10 to 23.22 g during treatment, while the body weight of mice in free gefitinib group keeps almost steady from ~ 23.28 to ~ 23.39 g possibly due to the loss of appetite, as shown in Fig. 5b.

Pathologic analysis

Gefitinib has been associated with hepatotoxicity, renal dysfunction and gastrointestinal perforation. To further confirm that FA-NPs could not only enhance therapeutic effect, but also reduce side effects and control inflammation to normal tissue, slices of major normal tissues (liver, kidney, and intestinal) are histologically analyzed by hematoxylin and eosin (H&E), as shown in Fig. 6. The slices of major organs of mice treated with FA-NPs show neglectable damage. In contrast, abnormal morphologies and obvious damages are found in the organ slices of mice treated with free gefitinib, suggesting the

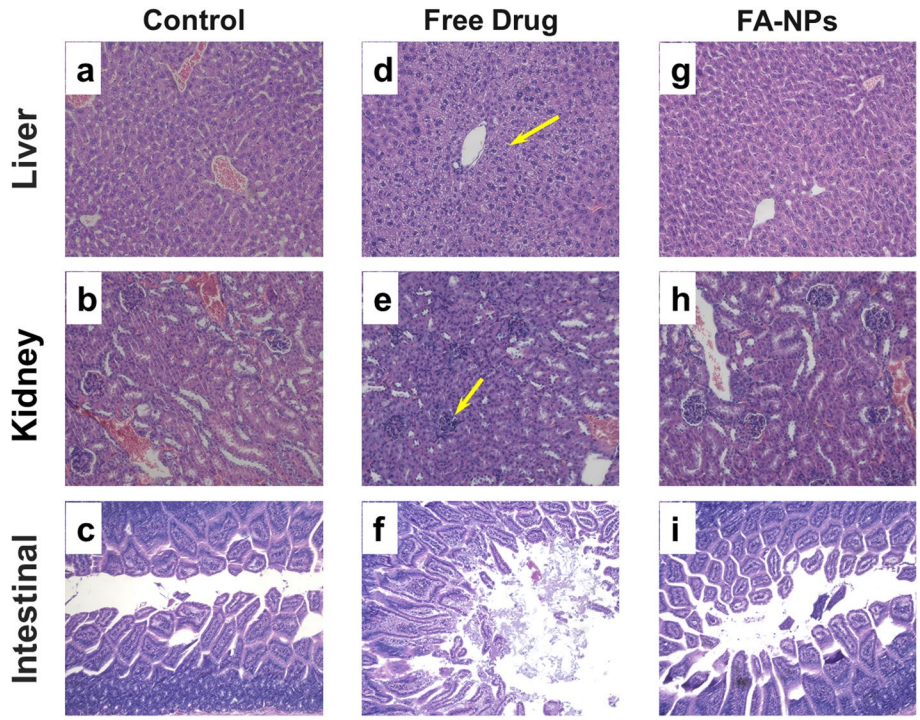

Fig. 6 H&E stained images of major organs in mice with different treatments: **a**–**c** PBS alone, **b**–**f** free gefitinib, and **g**-**i** FA-NPs

adverse events during long-term treatment of free gefitinib. These include: ballooning degeneration of hepatocyte cytoplasmic and enlargement of some liver cells nucleus in liver; mild proliferation of glomerular mesangial cell in kidney; local erosion of intestinal mucosa and proliferation of interstitial lymphocyte and plasma cells in intestinal. Together with the antitumor results from Fig. 5, we conclude that, gefitinib-loaded FA-NPs display a synergistic effect on NSCLC therapy, that is, enhanced inhibition on tumor and reduced side effects in normal tissues comparing with free drug.

Conclusion

In conclusion, we have prepared FA-NPs loaded with different EGFR-TKIs based on a continuous precipitation method FNP that enables rapid mixing of drug and polymer streams with anti-solvent. The fast process formulates kinetically controlled FA-NPs with well-defined particle size and properties. With gefitinib and FA-Dextran-*b*-PLA combination, we find that, the obtained gefitinib-loaded FA-NPs exhibit a hydrodynamic radius around 70 nm with a narrow distribution (PDI ~ 0.25) and a high DLC (15.9%). Moreover, the NPs formulation with FA ligand endows the EGFR-TKI an enhanced cellular uptake and proliferation inhibition of NSCLC cells, while lower cellular uptake and cytotoxicity in normal cell lines comparing with free drug. Correspondingly, in vivo results indicate that, gefitinib-loaded FA-NPs cause enhanced drug accumulation in tumor site and stronger inhibition on tumor growth, simultaneously associated with reduced drug collection and side effects in normal organs as liver and kidney. The FA-NPs delivery system fabricated by FNP here could not only improve the therapeutic

potential of EGFR-TKIs, but also eliminate their adverse effects, which is of interest and potential applications for a broad range of cancer therapy.

Methods

Materials

Dextran (Mn = 6 kDa) was purchased from Sigma Co., Ltd, and sodium cyanoborohydride (95%) was purchased from Acros Co. Ltd. Sodium tetraborate (99%), DL-lactide (DL-LA, 99%), benzyl alcohol (99.5%), acryloyl chloride (97%), stannous octoate (tin(II) bis(2-ethylhexanoate) ($Sn(Oct)_2$, 95%), triethylamine (99%), N,N-dicyclohexylcarbodiimide (DCC, 98%), 4-(dimethylamino) pyridine (DMAP, 98%) dimethyl sulfoxide (DMSO, 99.8%), gefitinib (98%), afatinib (98%), cisplatin (99%), and DMF (99.8%) were purchased from J&K Scientific Chemical Ltd. Ethylenediamine were chemically pure grade and purchased from Sinopharm Chemical Reagent Co, Ltd. Deionized water was obtained by a Milli-Q water purification system and was used in all experiments.

Synthesis of FA-Dextran-*b*-PLA

The Dex-*b*-PLA was synthesized according to our previous publication, as shown in Additional file 1: Fig. S1a–c (Wang et al. 2018a, b). Then folic acid group was introduced and grafted on dextran block, through an esterification reaction between γ-activated carboxyl group of FA and hydroxyl group of dextran with DMAP as an activator and DCC as a coupled agent, as shown in Additional file 1: Fig. S1d (Hao et al. 2013). Specifically, FA (0.46 g), DCC (0.2 g) and DMAP (0.13 g) were first dissolved in 25 mL anhydrous DMSO, and then stirred for 30 min under nitrogen atmosphere in dark at 30 °C in order to activate the carboxylic groups of FA. After adding 1.6 g Dex-*b*-PLA, the solution was stirred under nitrogen atmosphere for another 20 h at 30 °C. The solution was filtered to remove the precipitates, and then the filtrate was dialyzed against PBS (pH 7.4) to remove the unreacted FA following by dialysis against water (Spectra/Por6 MWCO 10 kDa, Spectrum Laboratories, Inc.). Finally, the solution was freeze-dried to obtain purified FA-Dextran-*b*-PLA. The final product was characterized by ^{1}H NMR on a Bruker AV400 NMR spectrometer in dimethyl-d^6 sulfoxide (DMSO-d^6). The ^{1}H NMR spectrum of FA-Dextran-*b*-PLA in DMSO-d^6 is shown in Additional file 1: Fig. S2. The peak at 3.0–5.0 ppm are attributed to Dextran protons; the peaks at 5.1 ppm, 1.4 ppm, and 7.3 ppm are attributed to PLA protons; the weak signals at 6.7 ppm (2H in phenylene), 7.6 ppm (2H in phenylene) and 8.7 ppm (1H in pteridine) are ascribed to FA protons. The FA graft degree in FA-Dextran-*b*-PLA is calculated by the peak area ratio of 7.6 ppm (2H in phenylene) to 3.1 ppm (2H in glucose unit) (Hao et al. 2013).

Preparation of FA-NPs

The FA-NPs were prepared by FNP via MIVM, as described in Scheme 1. Four inlets were connected to four syringes through Teflon tubing. One of the syringes was fed in drug solution (in DMF, 2 mg/mL, stream 1), one was FA-Dextran-*b*-PLA polymer solution (in PBS, 2 mg/mL, stream 2), and the remaining two were PBS buffer solution (stream 3 and 4). The four streams were mixed in the MIVM to yield FA-NPs, and flow velocities of streams were controlled by two syringe pumps (PHD 2000, Harvard Apparatus, Holliston, USA). The NP suspensions were then subjected to dialysis (dialysis bag,

Spectra/Por® MWCO 10KDa) against PBS buffer for 24 h to remove unencapsulated drug and DMF solvent. The out PBS buffer was refreshed every 8 h.

Characterization

The nanoparticle sizes (R_h) were measured by dynamic light scattering (DLS) method, which was performed in an ALV-CGS3 light scattering apparatus (ALV-GmbH, Langen, Germany), at a wavelength of 632.8 nm and fixed angle of 90°, at 25 °C. The CONTIN method is used to analyze the distribution of particle radius (Ding et al. 2020). For data processing, average and standard deviations were obtained from six duplicates with each acquisition times of 10 s. Nanoparticle morphology was observed on a TEM instrument (JEM-1400, JEOL, Tokyo, Japan) with an acceleration voltage of 100 kV. One drop of the nanoparticle solution was deposited on carbon-coated copper grid. The droplet was allowed to dry under ambient conditions.

The DLE and DLC were analyzed by a UV-1600 UV–Vis spectrophotometer (Shimadzu, Kyoto, Japan). In brief, a standard curve of drug was established by drug concentration and absorbance at 331 nm for gefitinib, 342 nm for afatinib, 310 nm for cisplatin, and then DLE and DLC were calculated according to Eqs. (1) and (2) separately:

$$\text{DLE (\%)} = \frac{\text{amount of drug in NPs}}{\text{total amount of feeding drug}} \times 100, \tag{1}$$

$$\text{DLC (\%)} = \frac{\text{amount of drug in NPs}}{\text{amount of drug} - \text{loaded NPs}} \times 100. \tag{2}$$

The release rates of drugs from NPs were investigated according to the following steps. Briefly, a dialysis membrane containing 2 mL of drug-loaded NPs was immersed in 20 mL of PBS solution (pH 7.4) at 37 °C. At the designed time point, 1 mL of the solution in outside medium was taken out and characterized by UV–vis spectrophotometer. Then the same volume of fresh buffer solution was added into the outside medium. The cumulative release rate was calculated according to Eq. (3):

$$\text{Cumulative release rate (\%)} = \sum \frac{10^{*}A_t}{A_0}{*}100\%, \tag{3}$$

where A_t is the absorbance of outside medium at time point t and A_0 is the absorbance of stock solution before dialysis.

Cell culture

The HCC827 NSCLC cell lines, HL7702 normal liver cell lines and 293 T normal kidney cell lines were purchased from the Institute of Cell Biology (Shanghai, China). They were propagated in T-75 flasks cultured at 37 °C under a humidified 5% CO_2 atmosphere in DMEM medium (GIBCO/Invitrogen, Camarillo, CA) supplemented with 10% fetal bovine serum (FBS, Biological Industry, Kibbutz Beit Haemek, Israel) and 1% penicillin–streptomycin (10000 U mL^{-1} penicillin and 10 mg mL^{-1} streptomycin, Solarbio Life Science, Beijing, China).

In vitro cytotoxicity assay

The cell cytotoxicity of NPs towards HCC827, HL7702 and 293 T cell lines were measured by cell counting kit-8 (Dojindo, Tokyo, Japan) according to the factory's instruction. Cells were plated in 96-well plates in 0.1 mL volume of DMEM medium with 10% FBS, at a density of $5*10^3$ cells/well. After incubation with added samples for 48 h, absorbance was measured at 450 nm with a microplate reader (Multiskan Sky-High, Thermo Fisher Scientific Inc., Waltham, USA).

Cell uptake

To evaluate the cell uptake of free gefitinib, NPs and FA-NPs, HCC827 cells or HL-7702 cells were seeded in a 6-well plate at a density of 2.0×10^4 cells per well in 2.0 mL of DMEM and cultured for 24 h. The medium was then replaced with 2.0 mL DMEM containing FA-NPs, NPs or free gefitinib at the same gefitinib concentration of 1 μmol/L and cultured for different time intervals: 3 h, 6 h, 9 h, 12 h, and 24 h. Specifically, free gefitinib is dissolved in DMEM containing 0.5% DMSO (*w*/*v*). The cells were treated with trypsin and washed with PBS at pH 7.4 twice again, and then the cells were re-suspended in 0.5 mL of PBS. Each sample was measured by using flow cytometry (CytoFLEX Flow Cytometer, Beckman Coulter Inc., USA) with filter NUV525 (Excitation at 355 nm and Emission at 525 nm) (Trummer et al. 2012; Zhang et al. 2017). The phagocytic ratio (%) is the ratio of gefitinib-containing cells to total cells.

Biodistribution assay

BalB/CA Nude Mice were purchased from Laboratory Animal Management Department of Shanghai Family Planning Research Institute (Shanghai, P. R. China). HCC827 tumor-bearing nude mice were intravenously injected with FA-NPs or free gefitinib (for both of FA-NPs and free drug, gefitinib dose are same: 5 mg per kg body weight; free gefitinib is dissolved in PBS containing 0.5% *w*/*v* DMSO). After different time intervals (1 h, 2 h, 4 h, 8 h, 12 h, 24 h), the mice were killedsacrificed to excise the blood, liver, kidney, and tumor. LC–MS (TSQ Altis, Thermo Fisher Scientific, Waltham, MA, USA) assessed the tissue distributions of gefitinib after digesting major internal organs of mice.

In vivo antitumor efficacy

HCC827 tumor-bearing nude mice (~100.0 mm^3 in size) were randomly divided into three groups ($n = 5$ per group) and intravenously injected with FA-NPs, free gefitinib, or PBS (for free gefitinib, gefitinib dose: 5.0 mg per kg, and free gefitinib is dissolved in PBS containing 0.5% *w*/*v* DMSO; for gefitinib-loaded FA-NPs, gefitinib dose: 5.0 mg per kg) every two days: day 1, 3, 5, 7, 9, 11 and 13. The length (L) and width (W) of each tumor were measured by calipers. The tumor volume (V) was calculated by the following Eq. (4):

$$\mathrm{V} = \frac{L \times W^2}{2}. \tag{4}$$

What's more, body weight was collected. On day 16, the mice were killed to excise the liver, kidney, intestine and tumor for H&E staining and histology analysis.

Statistical analysis

All results are expressed as the mean ± standard deviation. Statistical analyses are conducted employing SPSS (Statistical Product and Service Solutions) Statistics 25, to provide the *T*-test for significance and the calculation of p values. $p < 0.05$ is regarded as statistically significant: $^{*}p < 0.05$, $^{**}p < 0.01$, $^{***}p < 0.001$.

Abbreviations

NSCLC	Non-small-cell lung cancer
EGFR	Epidermal growth factor receptor
TKI	Tyrosine kinase inhibitors
NP	Nanoparticle
PLA	Polylactide
FA	Folate
FR	Folate receptor
FRα	Folate receptor α
FNP	Flash nanoprecipitation
MIVM	Multi-inlet vortex mixer
R_h	Hydrodynamic radius
PDI	Polydispersity index
DLE	Drug loading efficiency
DLC	Drug loading content
H&E	Hematoxylin and eosin

Supplementary Information

The online version contains supplementary material available at https://doi.org/10.1186/s12645-023-00199-2.

Additional file 1: Fig. S1. Synthesis of FA-Dextran-*b*-PLA. **Fig. S2**. ^{1}H NMR of FA-Dextran-*b*-PLA and dextran. **Table S1.** DLE and DLC of afatinib-loaded FA-NPs prepared by FNP and conventional precipitation. **Fig. S3.** TEM image of (a) gefitinib-loaded FA-NPs, and (b) cisplatin-loaded FA-NPs. **Fig. S4.** Cumulative release of (a) afatinib-loaded FA-NPs, (b) gefitinib-loaded FA-NPs, and (c) cisplatin-loaded FA-NPs, in PBS at pH 6.5 and pH 7.4, 37 °C. **Table S2.** Particle size, PDI, DLE and DLC of gefitinib-loaded NPs, the non-targeted NPs, prepared by FNP. **Fig. S5.** Flow cytometry analysis of the cellular uptake in HCC827 cells at different time intervals from 0 to 24 h: (a) free gefitinib; (b) NPs, without folate-ligand; (c) FA-NPs. Cellular uptake in HL7702 cells: (d) free gefitinib; (e) NPs, without folate-ligand; (f) FA-NPs; **Fig. S6.** Cytotoxicity to 293T normal kidney cell lines after incubation with free drug, NPs and FA-NPs for 48 h. **Table S3.** Biodistribution of gefitinib in vivo, concentrations of gefitinib in plasma and tissue in FA-NPs or free form, in HCC827-tumor-bearing nude mice after intravenous injection of FA-NPs or free gefitinib for designed time intervals. **Fig. S7.** UV-Vis spectra and normalized fluorescent emission spectra of gefitinib in DMF at 0.02 mg/mL, fluorescent excitation wavelength was 355 nm.

Acknowledgements
Not applicable for this study.

Author contributions
MW, JW and WB designed the research. J.W. and W.B. designed experiments and performed data analysis. MW, HH, ZZ, XC, YF, SC, ZQ performed most of the experiments. HH and DY organized figures and performed image analyses. MW, JW and WB co-wrote the paper. All authors listed edited and reviewed the manuscript. All authors read and approved the final manuscript.

Funding
This work was supported by "1000 Foreign Experts Program" (WQ20163100341), and National Natural Science Foundation of China (NSFC) for Young Scholars (21706074).

Availability of data and materials
All data generated or analyzed during this study are included in this published article.

Declarations

Ethics approval and consent to participate
All animal experiments conformed to the guidelines and standards of the animal welfare ethics committee and the animal laboratory of Shanghai Sixth People's Hospital.

Consent for publication
All authors agree with this publication.

Competing interests
The authors declare that they have no competing interests.

Received: 9 September 2022 Accepted: 18 April 2023
Published online: 05 May 2023

References

Akbulut M, Ginart P, Gindy ME, Theriault C, Chin KH, Soboyejo W, Prud'Homme RK (2009) Generic method of preparing multifunctional fluorescent nanoparticles using flash nanoprecipitation. Adv Funct Mater 19:718–725. https://doi.org/10.1002/adfm.200801583

Behzadi S, Serpooshan V, Tao W, Hamaly MA, Alkawareek MY, Dreaden EC et al (2017) Cellular uptake of nanoparticles: journey inside the cell. Chem Soc Rev 46:4218–4244. https://doi.org/10.1039/C6CS00636A

Bertran-Alamillo J, Cattan V, Schoumacher M, Codony-Servat J, Giménez-Capitán A, Cantero F et al (2019) AURKB as a target in non-small cell lung cancer with acquired resistance to anti-EGFR therapy. Nat Commun 10:1812. https://doi.org/10.1038/s41467-019-09734-5

Besford QA, Cavalieri F, Caruso F (2020) Glycogen as a building block for advanced biological materials. Adv Mater 32:1904625. https://doi.org/10.1002/adma.201904625

Blanco E, Shen H, Ferrari M (2015) Principles of nanoparticle design for overcoming biological barriers to drug delivery. Nat Biotechnol 33:941–951. https://doi.org/10.1038/nbt.3330

Breitenbach BB, Schmid I, Wich PR (2017) Amphiphilic polysaccharide block copolymers for pH-responsive micellar nanoparticles. Biomacromol 18:2839–2848. https://doi.org/10.1021/acs.biomac.7b00771

D'Addio SM, Prud'Homme RK (2011) Controlling drug nanoparticle formation by rapid precipitation. Adv Drug Deliver Rev 63:417–426. https://doi.org/10.1016/j.addr.2011.04.005

Devarakonda S, Govindan R (2019) Untangling the evolutionary roots of lung cancer. Nat Commun 10:2979. https://doi.org/10.1038/s41467-019-10879-6

Ding P, Huang J, Wei C, Liu W, Zhou W, Wang J et al (2020) Efficient and generic preparation of diverse polyelectrolyte nanogels by electrostatic assembly directed polymerization. CCS Chem 2:1016–1025. https://doi.org/10.31635/ccschem.020.202000354

Hao H, Ma Q, Huang C, He F, Yao P (2013) Preparation, characterization, and in vivo evaluation of doxorubicin loaded BSA nanoparticles with folic acid modified dextran surface. Int J Pharmaceut 444:77–84. https://doi.org/10.1016/j.ijpharm.2013.01.041

He Z, Santos JL, Tian H, Huang H, Hu Y, Liu L et al (2017) Scalable fabrication of size-controlled chitosan nanoparticles for oral delivery of insulin. Biomaterials 130:28–41. https://doi.org/10.1016/j.biomaterials.2017.03.028

Heigener DF, Kerr KM, Laing GM, Mok TSK, Moiseyenko FV, Reck M (2019) Redefining treatment paradigms in first-line advanced non-small-cell lung cancer. Clin Cancer Res 25:4881. https://doi.org/10.1158/1078-0432.CCR-18-1894

Hu H, Yang C, Li M, Shao D, Mao H, Leong KW (2021) Flash technology-based self-assembly in nanoformulation: fabrication to biomedical applications. Mater Today 42:99–116. https://doi.org/10.1016/j.mattod.2020.08.019

Jin M, Li G, Liu W, Wu X, Zhu J, Zhao D et al (2021) Cigarette smoking induces aberrant N6-methyladenosine of DAPK2 to promote non-small cell lung cancer progression by activating NF-κB pathway. Cancer Lett 518:214–229. https://doi.org/10.1016/j.canlet.2021.07.022

Johnson BK, Prud'Homme RK (2003a) Chemical processing and micromixing in confined impinging jets. AIChE J 49:2264–2282. https://doi.org/10.1002/aic.690490905

Johnson BK, Prud'Homme RK (2003b) Mechanism for rapid self-assembly of block copolymer nanoparticles. Phys Rev Lett 91:118301–118302. https://doi.org/10.1103/PhysRevLett.91.118302

Liu Y, Kathan K, Saad W, Prud'Homme RK (2007) Ostwald ripening of β-carotene nanoparticles. Phys Rev Lett 98:36102. https://doi.org/10.1103/PhysRevLett.98.036102

Liu Z, Ramezani M, Fox RO, Hill JC, Olsen MG (2015) Flow characteristics in a scaled-up multi-inlet vortex nanoprecipitation reactor. Ind Eng Chem Res 54:4512–4525. https://doi.org/10.1021/ie5041836

Liu K, Jiang X, Hunziker P (2016) Carbohydrate-based amphiphilic nano delivery systems for cancer therapy. Nanoscale 8:16091–16156. https://doi.org/10.1039/C6NR04489A

Liu Y, Yang G, Zou D, Hui Y, Nigam K, Middelberg APJ, Zhao C (2020) Formulation of nanoparticles using mixing-induced nanoprecipitation for drug delivery. Ind Eng Chem Res 59:4134–4149. https://doi.org/10.1021/acs.iecr.9b04747

Maemondo M, Inoue A, Kobayashi K, Sugawara S, Oizumi S, Isobe H et al (2010) Gefitinib or chemotherapy for non–small-cell lung cancer with mutated EGFR. New Engl J Med 362:2380–2388. https://doi.org/10.1056/NEJMoa0909530

Meador CB, Sequist LV, Piotrowska Z (2021) Targeting EGFR exon 20 insertions in non-small cell lung cancer: recent advances and clinical updates. Cancer Discov 11:2145–2157. https://doi.org/10.1158/2159-8290.CD-21-0226

Miao T, Wang J, Zeng Y, Liu G, Chen X (2018) Polysaccharide-based controlled release systems for therapeutics delivery and tissue engineering: from bench to bedside. Adv Sci 5:1700513. https://doi.org/10.1002/advs.201700513

Muralidharan R, Babu A, Amreddy N, Basalingappa K, Mehta M, Chen A et al (2016) Folate receptor-targeted nanoparticle delivery of HuR-RNAi suppresses lung cancer cell proliferation and migration. J Nanobiotechnol 14:47. https://doi.org/10.1186/s12951-016-0201-1

Murtuza A, Bulbul A, Shen JP, Keshavarzian P, Woodward BD, Lopez-Diaz FJ et al (2019) Novel third-generation EGFR tyrosine kinase inhibitors and strategies to overcome therapeutic resistance in lung cancer. Cancer Res 79:689. https://doi.org/10.1158/0008-5472.CAN-18-1281

Pi F, Binzel DW, Lee TJ, Li Z, Sun M, Rychahou P et al (2018) Nanoparticle orientation to control RNA loading and ligand display on extracellular vesicles for cancer regression. Nat Nanotechnol 13:82–89. https://doi.org/10.1038/s41565-017-0012-z
Popov AB, Melle F, Linnane E, González-López C, Ahmed I, Parshad B et al (2022) Size-tuneable and immunocompatible polymer nanocarriers for drug delivery in pancreatic cancer. Nanoscale 14:6656–6669. https://doi.org/10.1039/D2NR00864E
Saad WS, Prud'Homme RK (2016) Principles of nanoparticle formation by flash nanoprecipitation. Nano Today 11:212–227. https://doi.org/10.1016/j.nantod.2016.04.006
Santos JL, Ren Y, Vandermark J, Archang MM, Williford J, Liu H et al (2016) Continuous production of discrete plasmid DNA-polycation nanoparticles using flash nanocomplexation. Small 12:6214–6222. https://doi.org/10.1002/smll.201601425
Schatz C, Louguet S, Le Meins J, Lecommandoux S (2009) Polysaccharide-block-polypeptide copolymer vesicles: towards synthetic viral capsids. Angew Chem Int Ed 48:2572–2575. https://doi.org/10.1002/anie.200805895
Seidi F, Jenjob R, Phakkeeree T, Crespy D (2018) Saccharides, oligosaccharides, and polysaccharides nanoparticles for biomedical applications. J Control Release 284:188–212. https://doi.org/10.1016/j.jconrel.2018.06.026
Shi Y, Su C, Cui W, Li H, Liu L, Feng B et al (2014) Gefitinib loaded folate decorated bovine serum albumin conjugated carboxymethyl-beta-cyclodextrin nanoparticles enhance drug delivery and attenuate autophagy in folate receptor-positive cancer cells. J Nanobiotechnol 12:43. https://doi.org/10.1186/s12951-014-0043-7
Siegel RL, Miller KD, Fuchs HE, Jemal A (2022) Cancer statistics, 2022. CA A Cancer J Clin 72:7–33. https://doi.org/10.3322/caac.21708
Sousa De Almeida M, Susnik E, Drasler B, Taladriz-Blanco P, Petri-Fink A, Rothen-Rutishauser B (2021) Understanding nanoparticle endocytosis to improve targeting strategies in nanomedicine. Chem Soc Rev 50:5397–5434. https://doi.org/10.1039/D0CS01127D
Tan H, Wang N, Chan Y, Zhang C, Guo W, Chen F et al (2020) ID1 overexpression increases gefitinib sensitivity in non-small cell lung cancer by activating RIP3/MLKL-dependent necroptosis. Cancer Lett 475:109–118. https://doi.org/10.1016/j.canlet.2020.01.025
Tao J, Chow SF, Zheng Y (2019) Application of flash nanoprecipitation to fabricate poorly water-soluble drug nanoparticles. Acta Pharm Sin B 9:4–18. https://doi.org/10.1016/j.apsb.2018.11.001
Trummer BJ, Iyer V, Balu-Iyer SV, O'Connor R, Straubinger RM (2012) Physicochemical properties of epidermal growth factor receptor inhibitors and development of a nanoliposomal formulation of gefitinib. J Pharm Sci-US 101:2763–2776. https://doi.org/10.1002/jps.23180
Wang M, Yang N, Guo Z, Gu K, Shao A, Zhu W et al (2015) Facile preparation of AIE-active fluorescent nanoparticles through flash nanoprecipitation. Ind Eng Chem Res 54:4683–4688. https://doi.org/10.1021/acs.iecr.5b00501
Wang M, Lin S, Wang J, Liu L, Zhou W, Ahmed RB et al (2018a) Controlling morphology and release behavior of sorafenib-loaded nanocarriers prepared by flash nanoprecipitation. Ind Eng Chem Res 57:11911–11919. https://doi.org/10.1021/acs.iecr.8b02105
Wang M, Xu Y, Liu Y, Gu K, Tan J, Shi P et al (2018b) Morphology tuning of aggregation-induced emission probes by flash nanoprecipitation: shape and size effects on in vivo imaging. ACS Appl Mater Interfaces 10:25186–25193. https://doi.org/10.1021/acsami.8b08159
Yang X, Shi X, D'Arcy R, Tirelli N, Zhai G (2018) Amphiphilic polysaccharides as building blocks for self-assembled nanosystems: molecular design and application in cancer and inflammatory diseases. J Control Release 272:114–144. https://doi.org/10.1016/j.jconrel.2017.12.033
Yin H, Wang H, Li Z, Shu D, Guo P (2019) RNA micelles for the systemic delivery of anti-mirna for cancer targeting and inhibition without ligand. ACS Nano 13:706–717. https://doi.org/10.1021/acsnano.8b07948
York AW, Zablocki KR, Lewis DR, Gu L, Uhrich KE, Prud'Homme RK, Moghe PV (2012) Kinetically assembled nanoparticles of bioactive macromolecules exhibit enhanced stability and cell-targeted biological efficacy. Adv Mater 24:733–739. https://doi.org/10.1002/adma.201103348
Yuan R, Huang Y, Chan L, He D, Chen T (2020) Engineering EHD1-targeted natural borneol nanoemulsion potentiates therapeutic efficacy of gefitinib against nonsmall lung cancer. ACS Appl Mater Interfaces 12:45714–45727. https://doi.org/10.1021/acsami.0c08069
Zhang Z, Shi L, Wu C, Su Y, Qian J, Deng H, Zhu X (2017) Construction of a supramolecular drug–drug delivery system for non-small-cell lung cancer therapy. ACS Appl Mater Interfaces 9:29505–29514. https://doi.org/10.1021/acsami.7b07565
Zhang Y, Zhou Q, Wu Y (2019) Clinical management of third-generation EGFR inhibitor-resistant patients with advanced non-small cell lung cancer: current status and future perspectives. Cancer Lett 459:240–247. https://doi.org/10.1016/j.canlet.2019.05.044
Zhang J, Liu M, Zeng Z (2022) The antisolvent coprecipitation method for enhanced bioavailability of poorly water-soluble drugs. Int J Pharmaceut 626:122043. https://doi.org/10.1016/j.ijpharm.2022.122043
Zheng P, Ding B, Shi R, Jiang Z, Xu W, Li G et al (2021) A multichannel Ca^{2+} nanomodulator for multilevel mitochondrial destruction-mediated cancer therapy. Adv Mater 33:2007426. https://doi.org/10.1002/adma.202007426
Zhu Z (2013) Effects of amphiphilic diblock copolymer on drug nanoparticle formation and stability. Biomaterials 34:10238–10248. https://doi.org/10.1016/j.biomaterials.2013.09.015
Zhu Z, Xu P, Fan G, Liu N, Xu S, Li X et al (2019) Fast synthesis and separation of nanoparticles via in-situ reactive flash nanoprecipitation and pH tuning. Chem Eng J 356:877–885. https://doi.org/10.1016/j.cej.2018.09.103

Publisher's Note